Evaluation of Toxicity Ranking for Metal Oxide Nanoparticles *via* an *in Vitro* Dosimetry Model

Rong Liu,[†,‡,Δ] Haoyang Haven Liu,[†,⊥,Δ] Zhaoxia Ji,[†,Δ] Chong Hyun Chang,[†] Tian Xia,[†,§,Δ] Andre E. Nel,[*,†,§] and Yoram Cohen[*,†,‡,⊥]

[†]Center for Environmental Implications of Nanotechnology, [‡]Institute of the Environment and Sustainability, [⊥]Chemical and Biomolecular Engineering Department, and [§]Division of NanoMedicine, Department of Medicine, University of California, Los Angeles, California 90095, United States. [Δ]R. Liu, H. H. Liu, Z. Ji, and T. Xia contributed equally to the present study.

ABSTRACT It has been argued that *in vitro* toxicity testing of engineered nanoparticles (NPs) should consider delivered dose (*i.e.*, NP mass settled per suspension volume) rather than relying exclusively on administered dose (initial NP mass concentration). Delivered dose calculations require quantification of NP sedimentation in tissue cell culture media, taking into consideration fundamental suspension properties. In this article, we calculate delivered dose using a first-principles "particles in a box" sedimentation model, which accounts for the particle size distribution, fractal dimension, and permeability of agglomerated NPs. The sedimentation model was evaluated against external and our own experimental sedimentation data for metal oxide NPs. We then utilized the model to construct delivered dose—response analysis for a library of metal oxide NPs (previously used for hazard ranking and prediction making) in different cell culture media. Hierarchical hazard ranking of the seven (out of 24) toxic metal oxide NPs in our library, using EC_{50} calculated on the basis of delivered dose, did not measurably differ from our ranking based on administered dose. In contrast, simplified sedimentation calculations based on the assumption of impermeable NP agglomerates of a single average size significantly underestimated the settled NPs' mass, resulting in misinterpretation of toxicity ranking. It is acknowledged that *in vitro* dose—response outcomes are likely to be shaped by complex toxicodynamics, which include NP/cellular association, triggering of dynamic cell response pathways involved in NP uptake, and multiple physicochemical parameters that influence NP sedimentation and internalization.

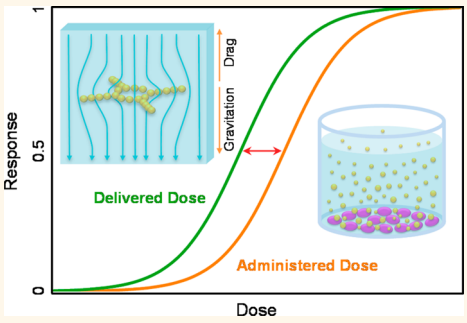

KEYWORDS: nanomaterial · dosimetry · sedimentation · nanotoxicology · dose—response

The applications of manufactured nanoparticles (NPs) in modern industrial and consumer products and processes are rapidly expanding[1,2] along with increased concern regarding the potential environmental health and safety (EHS) impact from NP exposures.[3−6] Various studies have identified that certain NPs can lead to adverse biological impacts,[7−12] *e.g.*, the possibility of oxygen radical production and oxidative stress that culminates in acute pulmonary inflammation by metal oxide NPs such as CoO, Co_3O_4, Ni_2O_3, Cr_2O_3, CuO, and ZnO.[13] Efforts are now mounting to ensure the development and application of safe-by-design engineered nanomaterials so as to avoid adverse environmental and human health impacts.[6,14−16] In this regard, *in vitro* toxicity screening is critical for characterizing the potential hazards of NPs and elucidating their toxicity mechanisms.[6,14,17−20] This includes use of high-throughput screening (HTS) approaches that enable rapid and cost-effective toxicity testing, hazard ranking, and prediction making of adverse health effects *in vivo*.[13,21−24]

In a typical *in vitro* screening platform for NP hazard assessment,[13,20,21] cells are plated at the bottom of tissue culture wells while NP suspensions are introduced at various particle concentrations, which are equivalent to what we regard as administered dose. Traditionally the administered dose, expressed as NP mass, number, or surface area per unit volume, is considered as the *in vitro* dose.[6,25] However, a number of studies have argued that cells at the bottom of a tissue culture well will be primarily impacted by NPs that have settled to the bottom of the plate.[26−32] Accordingly, there is an ongoing debate in the nanosafety community

* Address correspondence to yoram@ucla.edu, ANel@mednet.ucla.edu.

Received for review July 16, 2015 and accepted August 18, 2015.

Published online August 18, 2015
10.1021/acsnano.5b04420

regarding whether toxicity induced by NPs should be ascribed to delivered (*i.e.*, NP mass settled per the suspension volume) or administered (initial NP mass concentration) dose.[33−36] The outcome of this debate is relevant to the establishment of hazard ranking, which is often used for planning more expensive and time-consuming *in vivo* studies, in which the use of animals is often restricted.[13,31,32,37]

Methods to quantify NP sedimentation have been proposed on the basis of determining the concentration of NPs remaining in suspension after a given sedimentation period.[38] However, it is a formidable task to experimentally quantify the degree of sedimentation for an expanded range of NPs, which may require assays to be conducted in different cell types, different culture media, tissue culture plates with different dimensions, and different exposure times to generate comprehensive hazard profiles. Suitable models are therefore required to account for gravitational settling, particle diffusion, and the fractal nature of NPs.[30,39,40] Recently, predictions for NP sedimentation were investigated using the *in vitro* sedimentation, diffusion, and dosimetry (ISDD) model[36] that incorporated NP effective density measured by a volumetric centrifugation method (VCM).[34,35] These models have taken the simplified approach of using a single particle size (*e.g.*, average size), rather than accounting for the complete particle size distribution (PSD), to estimate the delivered dose, while also assuming nondraining NPs (*i.e.*, impermeable to solvent flow through the fractal NP agglomerate).[34−36] The above simplifications may have contributed, in part, to the reported deviation of ISDD model predictions of settled NP mass (*e.g.*, for silica, iron oxide, and polystyrene) from experimental data by "... as much as three-fold, but in most cases approximately two-fold ...".[36] It is known that, when suspended in cell culture media, NPs form agglomerates of various sizes, shapes, and fractal structures with significant porosity.[30,39−43] Such particle agglomerates can be partially draining, resulting in higher sedimentation velocity than impermeable aggregates of the same equivalent geometric or hydrodynamic size.[41−43] Moreover, it is noted that in the interpretation of dose−response profiles consideration of the PSD is important for NP toxicity predictions, as has been shown in previous studies of metal oxide NP toxicity.[37,44]

In order to account for the effect of agglomerate PSD and permeability on NP sedimentation and calculation of *in vitro* delivered dose, an improved sedimentation model was developed based on a "particles in a box" simulation approach.[45,46] This model considers the motion of particles by Brownian diffusion[47,48] and modified Stokes settling.[42] The model was validated based on experimental sedimentation measurements for NPs chosen from a group of 24 metal oxides, previously evaluated for *in vitro* hazard ranking and *in vivo* toxicity predictions.[13] We used this model to calculate the delivered dose and then compare the obtained *in vitro* hazard ranking relative to the ranking based on the administered dose, which is a critical step for selecting materials for further animal testing.

RESULTS AND DISCUSSION

Workflow for *in Vitro* NP Dosimetry Analyses. It has been argued that ranking of NP hazard through cellular screening should be established based on delivered (*i.e.*, NP mass settled per suspension volume) rather than administered (initial NP mass concentration) dose. Accordingly, in the present study we evaluated the impact of sedimentation (*i.e.*, NP settling) on hazard ranking, according to the workflow in Figure 1.

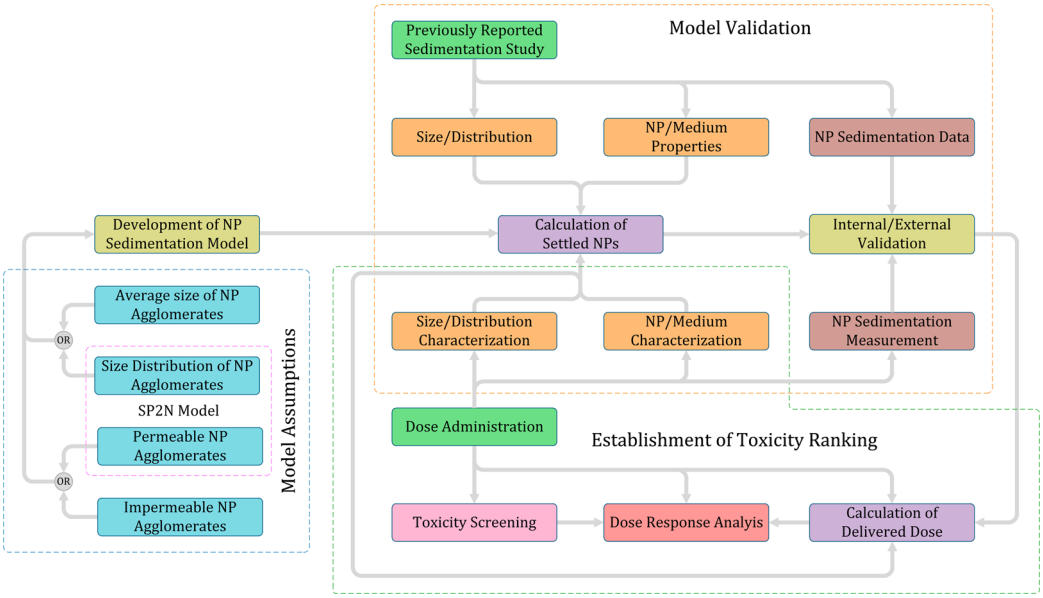

Figure 1. Workflow for *in vitro* NP dosimetry analysis.

TABLE 1. Summary of Physicochemical Properties of the NPs

				effective density	
property	primary size[a] (nm)	DLS size[b] (nm)	material density (g/mL)	BEGM (g/mL)	DMEM[c] (g/mL)
ZnO	22.6	149.20	5.60	1.35	1.25
Co_3O_4	10.0	181.41	6.11	1.34	1.37
CuO	12.8	202.29	6.31	1.48	1.50
CoO	71.8	142.99	6.44	2.54	2.39
Mn_2O_3	51.5	251.59	5.00	1.70	1.76
Cr_2O_3	193.0	464.39	5.22	2.19	2.34
Ni_2O_3	140.6	305.68	4.84	2.26	3.18

[a] TEM images of the NPs are provided in a previous study.[13] [b] DLS size was measured at an NP concentration of 100 mg/L. [c] The medium viscosities of DMEM[69] and BEGM[70] are 9.4 × 10^{-4} and 9.5 × 10^{-4} kg/m/s, respectively, while both have a medium density of 0.984 g/mL.

The analysis was carried out for seven metal oxide NPs (Table 1; Figure S3 in the SI), which we previously identified among a group of 24 metal oxide NPs, to be the materials that exhibit hazard potential based on redox chemistry and ability to generate oxidative stress.[13] A sedimentation model was developed to quantify the delivered dose, considering both the complete particle size distribution and the permeability of NP agglomerates. We will refer to this as the SP2N model. The SP2N model was validated by (i) previously reported experimental sedimentation data of CeO_2 NPs in deionized water,[49] and (ii) new experimental data for the sedimentation of selected metal oxide NPs in two commonly used cell culture media, bronchial epithelial growth medium (BEGM) and Dulbecco's modified media (DMEM). SP2N predictions were also compared with simplified sedimentation calculations, based on the assumption of the formation of impermeable NP agglomerates and an average agglomerate size. Subsequently, the validated SP2N model was applied to calculate the delivered NP doses for the seven metal oxide NPs (ZnO, Co_3O_4, CuO, CoO, Mn_2O_3, Cr_2O_3, and Ni_2O_3), referred to above. We have previously reported that these NPs exert dose-dependent pro-oxidative and pro-inflammatory effects in BEAS-2B and RAW264.7 cell lines, cultured in BEGM and DMEM, respectively.[13] The dose–response analyses for delivered and administered dose were subsequently used to assess the implications for *in vitro* hazard ranking, with a view to determining the necessity for further experimentation in animals and regulatory decision making.

Model Prediction and Experimental Measurements of NP Sedimentation. Sedimentation of NPs, for the purpose of calculating the delivered dose, was quantified *via* the SP2N model (Materials and Methods section). This model is premised on "particles in a box" simulation approach,[45,46] which tracks particle motion, as a result of gravitational settling[42] and Brownian motion.[47,48] Model predictions were compared with previously

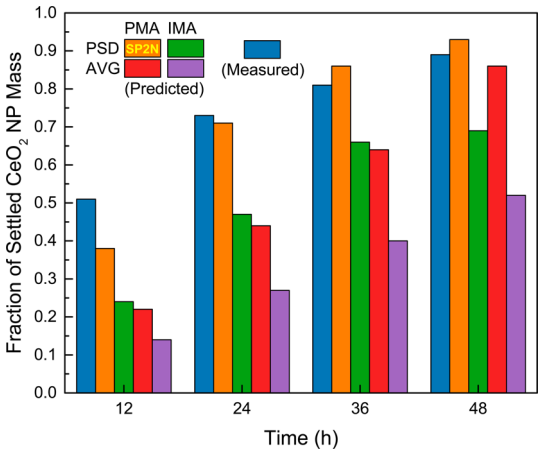

Figure 2. Comparison of reported experimental results[49] and model predictions for sedimentation of a 10 mg/L CeO_2 NP (20 nm) suspension in deionized water (neutral pH) based on complete particle size distribution (PSD) of (a) permeable (PMA), as in the SP2N model, or (b) impermeable (IMA) agglomerates, in addition to simplified calculations using average size (AVG) for (c) permeable and (d) impermeable agglomerates.

reported experimental NP sedimentation data in de ionized water and our own new results (based on ICP-OES measurements; Materials and Methods section) for selected NPs in BEGM and DMEM cell culture media. In addition, the relative trend of sedimentation behavior of the different NPs was also evaluated using a UV–vis measurement approach (Materials and Methods section).

SP2N model input parameters (Materials and Methods section) include basic NP properties (*i.e.*, material density, NP primary size, and agglomerate size distribution), geometrical parameters of NP agglomerates (fractal dimension and number of principle NP clusters), suspension properties (medium density and viscosity, NP concentration, and temperature), and medium depth. Model simulations yielded the time evolution of the settled fraction (in suspension) of the initial NP mass. The SP2N model was validated using experimental data for CeO_2 NPs (primary size of 20 nm; Table S1 and Figure S1 in the SI)[49] in deionized water (neutral pH). SP2N model predictions, which account for complete PSD and agglomerate permeability, were obtained for the mass fraction of settled CeO_2 NPs (relative to the initial mass in suspension) over a 12–48 h period (Figure 2). These calculations used a fractal dimension[36] of 2.45, with four NPs per primary cluster[43] (Figure S2, SI). The data were in good agreement with the sedimentation measurements,[49] with a percent relative deviation (*i.e.*, 100 × (measured − predicted)/measured) averaging ~9.7% (range of 2.7–25.5%). In contrast to the SP2N model predictions for CeO_2 NPs, predictions from a simplified model that uses the average size of permeable agglomerates were consistently lower than the sedimentation measurements[49] by a factor of up to 2.3 (Figure 2). Moreover, the predicted fraction of settled

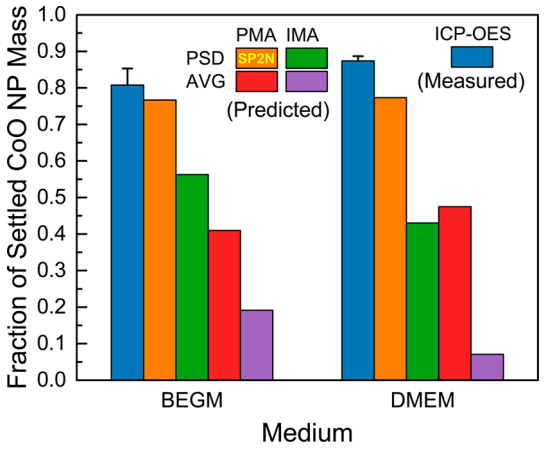

Figure 3. Comparison of experimentally determined fraction of settled CoO NPs (100 mg/L suspension in a 1.5 mL cuvette, 22 mm liquid depth) with model predictions based on complete particle size distribution (PSD) of (a) permeable (PMA), as in the SP2N model, or (b) impermeable (IMA) agglomerates, in addition to simplified calculations using average size (AVG) for (c) permeable and (d) impermeable agglomerates.

NP mass, when considering the agglomerates as impermeable, was 3.6-fold lower than the experimental values (Figure 2). The above underprediction of the settled fraction of NPs' mass is consistent with the reported level of underestimation of the ISDD model, which makes use of similar assumptions (*i.e.*, impermeable agglomerates of a single average size).[36] It is noted that the particle sedimentation velocity varies nonlinearly with particle diameter (Materials and Methods section). Thus, neglecting to account for the complete PSD and the large particles, which are likely to be found in the tail end of the distribution, could lead to a significant underestimation of the calculated fraction of settled NP mass. In addition, NP sedimentation will be further underestimated by regarding the agglomerates as impermeable, even when accounting for complete PSD (Figure 2). It is noted that previous studies have shown that permeable particles (of fractal structure) will settle faster than impermeable particles; thus, the assumption of impermeable agglomerates would also lead to underestimating the degree of particle settling.[41−43]

Validation of the sedimentation model under real tissue culture conditions was also conducted by using 24 h ICP-OES sedimentation data for CoO NPs in BEGM and DMEM culture media (Materials and Methods section), with a liquid depth of 22 mm in 1.5 mL cuvettes (Table 1 and Figure S3). SP2N model calculations were carried out for the fraction of settled CoO NP mass using the measured effective densities and complete PSD (Figure S3, SI), while also accounting for agglomerate permeability. Predictions of the fraction of settled NP mass (Figure 3) agreed well with the ICP-OES measurements with a relative deviation of 5.1−11.5% below the measurements. It is noted that the calculated fraction of settled NP mass based on the simplified model (*i.e.*, assuming impermeable agglomerates of a single average size) was lower than the experimental ICP-OES results by a factor of 1.8−2.0 and 4.2−12.4, respectively (Figure 3). Additional ICP-OES sedimentation measurements (Materials and Methods section) for 100 mg/L suspensions of Ni_2O_3, Cr_2O_3, and Mn_2O_3 NPs in DMEM, using the same 1.5 mL cuvettes (22 mm liquid depth), also demonstrated a significant fraction of settled mass (>0.96) over the typical 24 h toxicity screening interval (Figure S4, SI). SP2N model predictions also closely matched these ICP-OES measurements with a relative deviation up to 7.3% (Figure S4, SI). It is noted that for NPs that exhibit measurable solubility a decrease in particle size is expected, thus resulting in lesser NP settling relative to insoluble particles of the same PSD and initial mass concentration. Indeed, as shown for the sedimentation of ZnO (Figure S4, SI), which has been reported to have measurable aqueous solubility,[13] the measured fraction of settled NP mass (0.12) was below model predictions (0.17).

Finally, we note that the more approximate experimental analysis *via* UV−vis measurements (Materials and Methods section) for an extended set of 24 metal oxide NPs (Figure S5, SI) was also consistent with the general trend of relatively high NP sedimentation fraction. However, UV−vis measurements are affected by the agglomerate size distribution, as well as NP dissolution; thus, such measurements should be regarded as indicative of trends rather than providing precise quantitative measures of the concentration of NPs in suspension.[50]

Toxicity Ranking of Metal Oxide NPs per Administered and Delivered Doses. In order to evaluate the impact of metal oxide NP sedimentation on hazard ranking, the validated sedimentation model was applied to the seven metal oxides (Table 1; Figure S3 in the SI) that showed hazard potential (Figure 4) during the study of a group of 24 NPs.[13] Briefly, the hazard ranking was carried out based on dose−response analysis, derived from performance of ATP, LDH, and MTS viability assays in BEAS-2B and RAW264.7 cell lines (Table 1). The administered dose in these experiments ranged from 0.4 to 100 mg/L (Figure S6, SI), and the liquid tissue culture depth was 3.15 mm in each plate well. Calculations of the delivered doses were carried out for the seven metal oxide NPs to compare changes in hazard ranking (Figures S6−S8, SI). The delivered dose (C_d, defined as the NP mass settled per the medium volume)[35,36] was expressed as $C_d = \alpha C_a$, where α is the model calculated fraction of settled NPs (Figure 5) and C_a identifies administered NP dose.

Hazard ranking of the seven metal oxide NPs was assessed on the basis of EC_{50} (Figure 6) and Hill slope (Figure 7) of the dose−response curves[37,51] that were calculated from the commonly used log−logistic

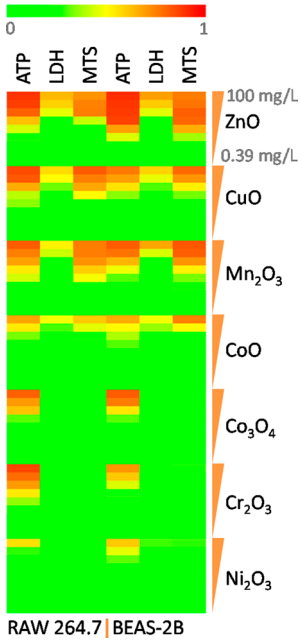

Figure 4. Toxicity heatmap of seven metal oxide NPs that can impact cell viability at different administered dose levels. The reduction of RAW 264.7 and BEAS-2B cell viability was measured through ATP, LDH, and MTS assays, which were further normalized as percent of control (POC ∈ [0, 1]). Increased POC values indicate higher toxicity.

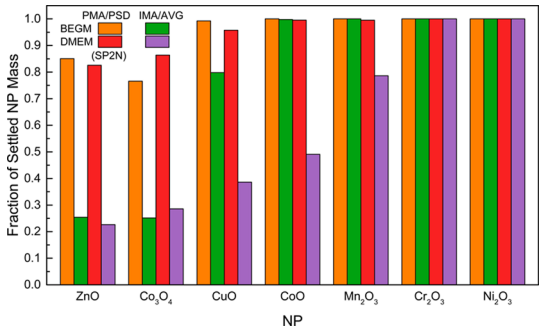

Figure 5. Calculated fraction of settled NP mass (100 mg/L suspension in BEGM or DMEM culture media) in the wells of a 96-well plate (3.15 mm medium depth). The calculations were performed according to the SP2N dosimetry model, based on the complete particle size distribution (PSD) of permeable agglomerates (PMA), and by a simplified analysis using average size (AVG) and assuming an impermeable agglomerate (IMA).

dose–response model[37,51] (Materials and Methods section). The comparative ranking, based on EC_{50} calculations, did not show a change in the toxicity ranking by delivered *vs* administered dose (Figure 6), except for the higher EC_{50} for ZnO relative to CuO in RAW264.7 cells. We note, however, that the delivered EC_{50} values (10.3 and 12.7 mg/L) for ZnO and CuO differed by only 2.4 mg/L, which falls within the range of experimental uncertainty (Figure 6). Therefore, one should not assert that the above difference is indicative of a change in hazard ranking for the ZnO and CuO NPs. It is also important to note that, with the exception of ZnO data for both cell lines and the Co_3O_4 data for the ATP assay in the BEAS-2B cell line, the actual EC_{50} values (Figure 6), based on the administered or SP2N model calculations, remained essentially unchanged for all other NPs. The above results are not surprising given the nearly complete sedimentation (*i.e.*, $\alpha > 0.96$) of these NPs in the shallow plate wells (Figure 5) and the close matching of administered and delivered doses.

In contrast with the above, analysis premised on the assumption of impermeable agglomerates of average size (*i.e.*, as assumed by the ISDD model),[35] the EC_{50} toxicity ranking of delivered dose was noticeably altered (Figure 6). This change in ranking is a consequence of the significant underestimation of the fraction of settled mass for the ZnO, CuO, CO_3O_4, and CoO NP (Figure 5) suspensions in both DMEM and BEGM. For example, for the LDH assay, performed in BEAS-2B cells, the EC_{50} of Co_3O_4 was less than that of CoO. This toxicity ranking is consistent with previous analysis[35] based on the ISDD model (*i.e.*, which does not account for the complete PSD and agglomerate permeability). In contrast, toxicity ranking on the basis of either administered dose or SP2N delivered dose calculations demonstrated that EC_{50} for CoO was higher than for Co_3O_4. Clearly, approximate NP sedimentation models can lead to erroneous estimates of the fraction of settled NP mass (Figure 5) and thus misinterpretation of toxicity ranking on the basis of delivered dose (Figure 6).

It could be argued that different toxicity ranking criteria (*e.g.*, EC_{50}, dose–response Hill slope,[37,51] or benchmark dose) may not necessarily be consistent with each other and that it is important to evaluate more than a single criterion.[50] For instance, when the Hill slope of the dose–response curve (Figure 7) is used to rank NP toxicity, we observe a left-shift of the delivered dose–response curves (Figures S7 and S8, SI) relative to the administered dose-response curves (Figure S6, SI). Therefore, EC_{50} scales by an α-factor when the dose–response curves are constructed based on delivered *vs* administered dose. However, the Hill slope,[37,51] which is also an important toxicity parameter (or potency),[37,52] remained unchanged, irrespective of whether one utilizes the administered or delivered dose (Figure 7).

It is tempting to argue that delivered dose should be the dosimetry metric of choice given that ultimately NPs will deposit onto cells at the bottom of a plate. However, one must consider that particle/cellular interactions are complex and dynamic processes that involve cell/particle association,[53,54] cellular uptake,[55,56] subcellular translocation,[57] and bioprocessing,[58,59] which ultimately determines the toxicity outcomes. Here it is pertinent to note, as illustrated in the MTS assay (Figure S9), that the toxicological response does not appear to increase progressively in the higher dose range (200–500 mg/L), supporting the argument that dose (delivered or administered) is not the only

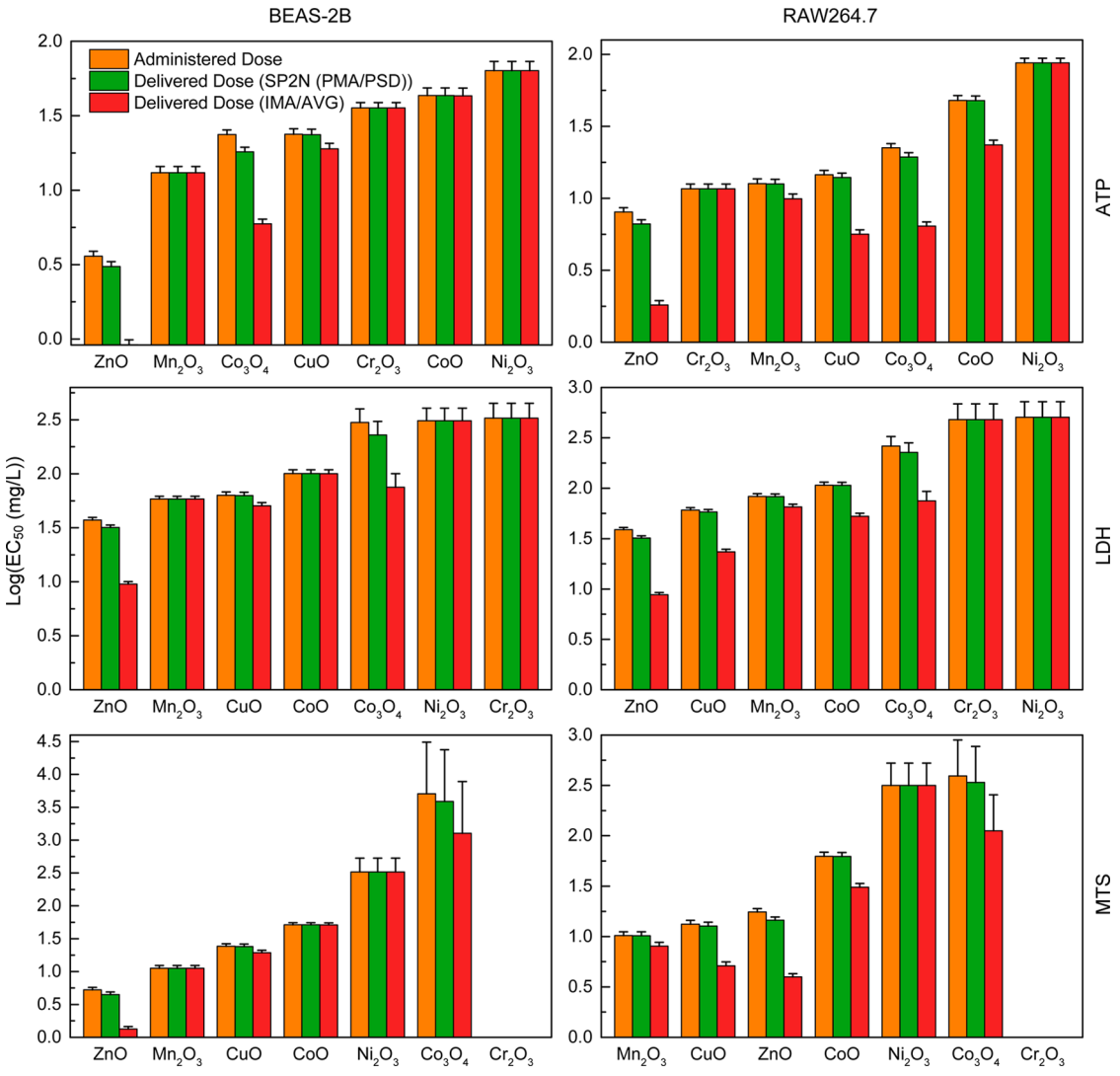

Figure 6. Log(EC_{50} (mg/L)) for NPs obtained from dose–response analyses, using either administered or delivered dose. Delivered dose was calculated by the SP2N dosimetry model based on the complete particle size distribution (PSD) of permeable agglomerates (PMA) and by a simplified analysis using average size (AVG) and assuming impermeable agglomerates (IMA). (Note that dose–response results for Cr_2O_3 in the MTS assay did not reach a 50% viability reduction during the 24 h experimental exposure period.)

governing factor. One should also recognize that cellular toxicity is a dynamic process with its own kinetics, as demonstrated by the multiparametric high-throughput assay for oxidative stress performed on the same materials.[13] Thus, it should not be surprising to discover that the toxicological readout in the cell viability assays after 24 h represents a dynamic series of cellular responses that evolve through different phases and stages.[13,37,60,61] We also note that in the case of soluble metal oxide NPs (*e.g.*, ZnO) their cellular toxicity has been linked to the NP dissolution release and mobility of the metal cation.[13,37] Clearly, the issue of establishing the most appropriate dosimetry is of importance and would most likely need to be established on the basis of the toxicity mechanisms that are engaged by specific material compositions and variation of physicochemical characteristics that can dynamically change the outcome.[62] Moreover, *in vitro* NP cellular dose–responses should consider NP size distribution, interaction of NPs with various species in the exposure media (*e.g.*, proteins[53]), and their influence on toxicokinetics.

CONCLUSIONS

It has been argued that delivered dose rather than administered dose should be considered in *in vitro* toxicity testing of engineered NPs. Accordingly, the present study presents a comparative analysis of toxicity ranking on the basis of administered and delivered dose–response for a library of 24 metal oxide NPs in different cell culture media. Delivered dose calculations were conducted using a first-principles "particles in a box" sedimentation model taking into consideration fundamental suspension properties. The model, which accounts for the particle size distribution, fractal dimension, and permeability of agglomerated NPs,

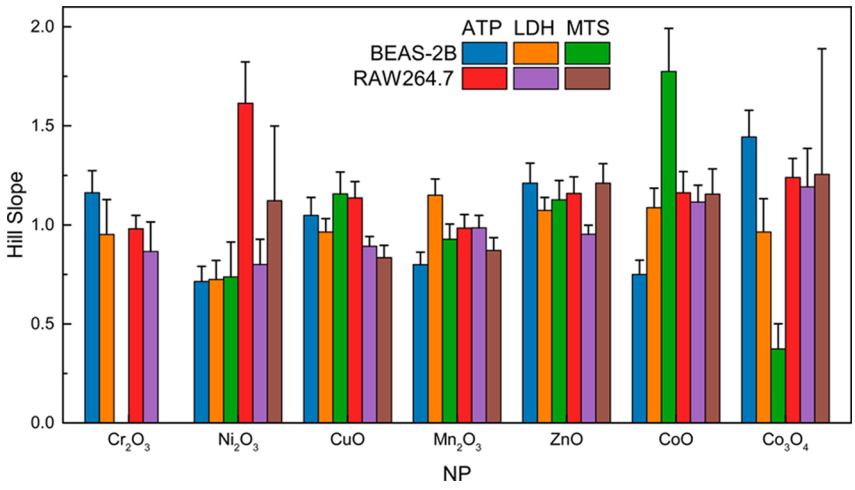

Figure 7. Hill slope of the individual NPs based on the administered dose−response curves for the ATP, LDH, and MTS assays for the BEASE-2B and RAW264.7 cells, which were exposed to the indicated metal oxide NPs at an administered dose range of 0.4−100 mg/L.

was evaluated against external and our own experimental sedimentation data for metal oxide NPs. Detailed dose−response analysis revealed that hierarchical hazard ranking of the seven toxic metal oxide NPs in our data set, using EC_{50} calculated on the basis of delivered dose, was similar to ranking based on administered dose. This corrects the misinterpretation in toxicity ranking through the use of simplified sedimentation calculations that assume impermeable NP agglomerates of a single average size, which results in significant underestimation of the mass of settled NPs. Notwithstanding the above results, it is important to recognize that *in vitro* dose−response outcomes could result from complex toxicodynamics, which include triggering of dynamic cell response pathways involved in NP uptake, NP/cellular association, and various physicochemical factors that impact NP sedimentation and cellular response.

MATERIALS AND METHODS

The workflow for *in vitro* NP dosimetry analysis is summarized in Figure 1. The simulation model for NP sedimentation was developed based on the fundamental principle of Stokes settling velocity, using either average NP size or size distribution and also considering permeable or impermeable NP agglomerates. The developed model was evaluated against CoO NP sedimentation measured in BEGM and DMEM culture media, as well as previously reported sedimentation data for CeO_2 NPs in deionized water.[49] In addition, NP sedimentation model was also validated through the use of complementary sedimentation measurements for selected metal oxide NPs. Dose−response analyses were then conducted to compare the hazard ranking of seven potentially hazardous metal oxide NPs based on administered dose as well as the calculated delivered dose.

Acquisition of NP Metal Oxide Toxicity Data. We utilized a comprehensive data set for 24 metal oxide NPs, previously obtained by conducting MTS, ATP, and LDH assays with RAW 264.7 and BEAS-2B cells.[13] This library of NPs was commercially purchased or synthesized in-house. BEAS-2B cells were cultured in BEGM medium (Lonza, Walkersville, MD, USA), while RAW 264.7 cells were cultured in DMEM medium (containing 10% fetal calf serum, 100 U/mL penicillin, 100 mg/L streptomycin, and 2 mM L-glutamine).[13] Details of the media compositions are provided in Table 1. Briefly, cell cultures were cultured overnight by plating 10 000 cells in 100 μL of medium in each well of a 96-multiwell black plate (Costar, Corning, NY, USA). The medium was removed and cells were treated for 24 h in 100 μL of a series of NP suspensions, each added to achieve final concentrations of 0.4, 0.8, 1.6, 3.2, 6.3, 12.5, 25, 50, and 100 mg/L. These are also regarded as the administered doses. For the three assays, triplicates of NPs and negative controls were used, while for LDH a reference positive control was provided by the response of cells treated by 0.01% Trition-100.[13] The MTS data set also included higher doses (up to 500 mg/L) to assess if that would lead to further toxicity. All the screening results collected for the MTS, ATP, and LDH assays were normalized and expressed as percent of control (POC), over the range of 0 to 1.[13,37]

Particle Size Characterization and Density of NP Agglomerates. The size distributions of the hazardous NPs (Table 1) were determined by dynamic light scattering (DLS) in BEGM and DMEM culture media for particle suspensions of 100 mg/L. DLS measurements were carried out at 298 K using a Brookhaven ZetaPALS dynamic light scattering analyzer with a wavelength of 657.0 nm and a detection angle of 90°. The sizes of the 17 nontoxic NPs were previously determined as reported elsewhere.[13]

The NP agglomerate density was determined following a previously established approach.[35] Briefly, a 1 g/L stock solution of each material was prepared, which was further diluted with cell culture media in a TPP packed cell volume tube (Techno Plastic Products, Trasadingen, Switzerland) to prepare a 100 mg/L NP suspension.[38] A 1 mL amount of the suspension was subsequently centrifuged at 4000*g* for 1 h to obtain a pellet of the agglomerated NPs. The pellet volume, V_{pellet}, was measured in triplicate for each sample and used to calculate the effective agglomerate density, *i.e.*, $\rho_{EV} = (\rho_{media}V_{media} + \rho_{NP}V_{NP})/(V_{pellet} \times SF)$, where ρ_{media} and ρ_{NP} are the densities for the cell culture media and NPs, respectively, and V_{media} and V_{NP} represent the volumes of the cell culture media and NPs, respectively. The medium density was determined by weighing 50 mL of freshly prepared culture medium in a disposable centrifuge tube. The stacking factor (SF) was taken to be 0.634 (random close packing) as reported in previous studies.[63]

Measurement of Settled NPs. Sedimentation measurements, quantified in terms of the mass of settled NPs, were obtained for ZnO, CuO, Mn_2O_3, CoO, Co_3O_4, Cr_2O_3, and Ni_2O_3 NPs by determining the metal concentration in suspension initially and

subsequently in the supernatant after a sedimentation period of 24 h. The procedure involved preparation of a stock suspension of 5 mg/mL, which was used subsequently to prepare 1 mL of a 100 mg/L NP suspension. NPs from the 1 mL of the suspension (in a 1.5 mL cuvette) were allowed to settle for 24 h. Subsequently, 0.9 mL of the "supernatant" was withdrawn and acid digested at 95 °C overnight in 10 mL of concentrated nitric acid (HNO_3, 65−70%, Trace Metal grade) in a HotBlock (SC100, Environmental Express). The dried sample was extracted into 8 mL of 2% diluted nitric acid and heated to 80 °C for 3 h. After cooling to room temperature, 2% nitric acid was added to the sample to reach a total volume of 8 mL. The metal content in the above samples was determined by ICP-OES analysis (ICPE-9000, Shimadzu, Japan) in nine replicates. The initial metal concentration of the suspension was also determined by acid digestion and ICP-OES using 0.2 mL of the suspension sample.

In addition to the sedimentation measurements, *via* ICP-OES analysis, we also evaluated the NP suspension stability by using a UV−vis spectrophotometer (SpectraMax M5e microplate reader, Molecular Devices) equipped with a 1.5 mL quartz cuvette. The particle absorbance at 500 nm, with material suspended in BEGM or DMEM in a 1 mL cuvette, was monitored as a function of time for 24 h. A linear calibration of the absorbance *vs* the NP concentration was obtained for each material to calculate suspension stability.

NP Sedimentation Model. In order to estimate the delivered NP dose *in vitro*, a sedimentation model that considers both particle size distribution and agglomerate permeability of NP (SP2N) was developed based on the "particles in a box" simulation approach.[45,46] Particle motion in this model considers both Brownian diffusion[47,48] and gravitational settling.[42] The SP2N model was used to calculate the fraction of the initial NP mass (in the suspension) that settles over a given time, t, to the bottom of the well. Accordingly, the delivered dose can be calculated according to eq 1:

$$f_t^s = \frac{\sum_{i\in S} m_i}{\sum_{i=1}^{N} m_i} \tag{1}$$

where $i = 1 \ldots N$ represents the initial agglomerates in the simulation box with S denoting the set of the settled NP agglomerates, and m_i (kg) is the mass of NP agglomerate i (*i.e.*, $m_i = \rho_{e,i}\pi d_i^3/6$, in which $\rho_{e,i}$ and d_i are the particle effective density and diameter, respectively).

The modeling approach for NP sedimentation is based on a simulation of particles in a box containing a number of (typically 10^5) randomly distributed NPs. Basic model parameters include NP properties (*i.e.*, NP primary size and material density), geometrical particle parameters (size distribution, fractal dimension, number of principle agglomerate clusters), suspension properties (NP concentration, temperature, and medium density and viscosity), and medium depth. Given these input parameters, the simulation starts with a set of N NPs, with diameters sampled from a specified PSD, obtained through experimental measurements of the NP suspensions in the liquid medium under evaluation. The above sampling can be accomplished, for PSDs that are described by an analytical function (*e.g.*, normal or log-normal distribution), based on the generation of N random numbers from the specified PSD. Alternatively, for PSDs that are in a discretized form (*i.e.*, an array of size bins with corresponding particle number frequencies), the sampling of NP diameters can be carried out by first allocating n_l particles to each bin, l, based on the above specified frequencies, such that $n_l = Nf_l^b/\sum_{l=1}^{M} f_l^b$, where f_l^b is the frequency for bin l, and $l = 1 \ldots M$ denoting the size bins. Subsequently, for each bin l, the particle sizes of the n_l particles are obtained by generating m_l uniformly distributed random numbers between the minimum and maximum size of the bin. The simulation time (t_{final}) is divided into n equal time steps (typically 100), whereby at each time step the vertical positions of all NP agglomerates in suspension are updated based on the particle displacement due to Brownian diffusion and gravitational settling. The vertical travel distance for particle i (Δz_i) is determined at each time step ($\Delta t = t_{final}/n$) for all particles in the simulation box according to

$$\Delta z_i = \Delta z_{S,i} + \Delta z_{B,i} \tag{2}$$

where $\Delta z_{S,i}$ and $\Delta z_{B,i}$ are the gravitational settling and diffusion traveling distances in the vertical direction, respectively, for NP agglomerate i (*i.e.*, relative to their vertical position in the previous time step). As lateral movements do not contribute to vertical repositioning of particles, the vertical particle travel distance attributed to Brownian diffusion, $\Delta z_{B,i}$ (positive or negative for upward or downward movement, respectively), is estimated as the vertical travel distance determined based on a random number sampled from a normal distribution with $\mu = 0$ and $s = \sqrt{2D_i\Delta t}$ such that[47,48]

$$\Delta z_{B,i} \approx \mathcal{N}(0, 2D_i\Delta t) \tag{3}$$

in which D_i is the Brownian diffusivity determined from[47,48]

$$D_i = \frac{kT}{6\pi\eta r_i} \tag{4}$$

where k is the Boltzmann constant, T is the medium temperature, η is the medium viscosity, and r_i is the radius of particle i.

The gravitational sedimentation distance ($\Delta z_{S,i}$, negative for downward movement) is calculated as

$$\Delta z_{S,i} = v_{S,i}\Delta t \tag{5}$$

in which $v_{S,i}$ is the modified Stokes settling velocity that accounts for the agglomerate porosity and permeability (eq 6). At each time step, particles with vertical positions below the bottom boundary of the box (*i.e.*, $z_{i,\tau} = z_{i,\tau-1} + \Delta z_i \le 0$, where $z_{i,\tau}$ and $z_{i,\tau-1}$ are the particle vertical positions at the τth and $(\tau - 1)$th time step, respectively) are considered to have settled to the bottom of the box (*i.e.*, the *in vitro* plate well) and no longer present as suspended particles (*i.e.*, in the suspension).

NPs that readily agglomerate in aqueous suspensions typically exist as fractal structures. These fractal agglomerates may be partially draining, as has been discussed in a number of studies on gravitational settling of complex agglomerates.[41−43] These studies have demonstrated that the assumption of impermeable agglomerates can lead to significant underestimation (by up to an order of magnitude and higher) of the agglomerate settling velocity. Accordingly, modifications to the classical Stokes settling velocity have been proposed, whereby the correction factor takes the form[42]

$$\Gamma = \frac{v_{s,i}^{\text{permeable}}}{v_{s,i}^{\text{impermeable}}} = \frac{\xi_i}{\xi_i - \tanh(\xi_i)} + \frac{3}{2\xi_i^2} \tag{6}$$

where $v_{s,i}^{\text{permeable}}$ and $v_{s,i}^{\text{impermeable}}$ are the settling velocities of a permeable agglomerate and impermeable sphere of the same diameter, respectively, and ξ_i is the dimensionless permeability of the fractal agglomerate i. The Stokes settling velocity for an impermeable sphere is expressed as

$$v_{s,i}^{\text{impermeable}} = \frac{(\rho_{e,i} - \rho_f)gd_i^2}{18\eta} \tag{7}$$

in which $\rho_{e,i}$ and d_i are the particle effective density and diameter, respectively, ρ_f is the fluid density, g is the gravitational constant, and η is the medium viscosity. Since NP agglomerates have a fractal porous structure, their effective density $\rho_{e,i}$, which is lower relative to that of a solid sphere of the same diameter, can be estimated from

$$\rho_{e,i} = \rho_p(1 - \varphi_i) + \rho_f\varphi_i) \tag{8}$$

where ρ_p is the NP material density and φ_i is the dimensionless NP porosity related to the fractal dimension, d_f, by

$$\varphi_i = 1 - (d_i/d_p)^{d_f - 3} \tag{9}$$

where d_p is the primary NP diameter. It is noted that if an experimental measurement of the average effective density

of the NP agglomerates in suspension is available, the fractal dimension may be extracted from eqs 8 and 9.

Various expressions have been proposed for the permeability of a fractal agglomerate such as the Carman–Kozeny,[64] Brinkman,[65] and Happel[66] equations. However, it has been reported that the above permeability expressions are based on the assumption of primary particles and pores that are uniformly distributed; this simplification is unrealistic for fractal agglomerates, and following such a correction to the settling velocity still results in significant underestimations (by up to a factor of 2) of the settling velocity.[43,67,68] In order to overcome the above limitation, modification of the above permeability expression has been proposed,[43] according to which an agglomerate is taken to be composed of a few ($\lesssim$10) principle clusters (of primary particles) that thus have larger pores between the principle clusters.[43] Among the various proposed modified permeability expressions, the Brinkman and the Happel equations were assessed to be most suitable for fractal agglomerates over a wide range of fractal dimension (d_f = 1.7–2.5).[43] For example, the modified dimensionless permeability based on the modified Brinkman equation, which was used in the present work, is given as[43]

$$\xi_i = 4.2\left(\frac{n}{c}\right)^{1/d_f}\left[3+\frac{4}{c}\left(\frac{n}{c}\right)^{3-d_f/d_f}-3\sqrt{\frac{8}{c}\left(\frac{n}{c}\right)^{3-d_f/d_f}-3}\right]^{-1/2} \quad (10)$$

in which n is the number of principle clusters (typically $n \geq 4$),[43] c is a packing coefficient reported to be in the range 0.15–0.25,[43] and d_f is the fractal dimension. The above expression can then be used in eq 6 to calculate the settling velocity for the NP agglomerates.

Dose–Response Analysis. In order to establish toxicity metrics based on administered and delivered NP dose, dose–response analyses were conducted *via* the commonly used log–logistic model:[37,51]

$$y = 1/(1+10^{s(\log_{10}EC_{50}-\log_{10}x)}) \quad (11)$$

In the above model, x and y identify the NP dose and response, respectively, while the shape of the log–logistic curve is dictated by the EC_{50} and Hill slope (s).[51] Here it is noted that the dose (x) is either the administered or delivered dose. The latter can be expressed in terms of either the deposited mass per unit volume or other suitable dose metrics (*e.g.*, surface area) given the PSD tracked by the SP2N model. According to the log–logistic model, if the dose (x) is scaled by a factor of α ($\leq$1), then the fitted dose–response curve will shift horizontally to the left by a distance of $\log_{10}(\alpha)$, while its shape will remain unchanged (Figure 8). In the present work, dose–response

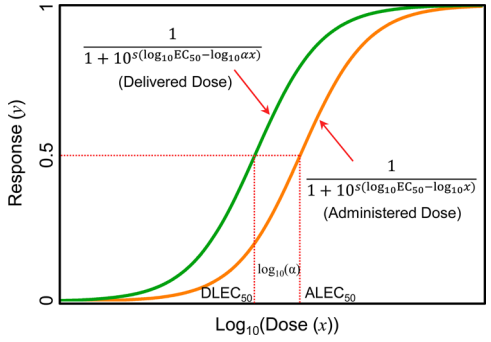

Figure 8. Illustration of log–logistic dose–response curves based on administered and delivered dose. (Note: Dose (x) refers to NP of type x and Response (y) is the normalized specific assay response with respect to the control.)

analyses were accomplished using OriginPro 9 (OriginLab, Northampton, MA, USA) using the response data of all triplicates (*i.e.*, three data points for each NP at each administered dose) to avoid loss of information.

Conflict of Interest: The authors declare no competing financial interest.

Acknowledgment. This material is based upon work supported by the National Science Foundation and the Environmental Protection Agency under Cooperative Agreement Number DBI-0830117. Any opinions, findings, and conclusions or recommendations expressed in this material are those of the author(s) and do not necessarily reflect the views of the National Science Foundation or the Environmental Protection Agency. This work has not been subjected to EPA review, and no official endorsement should be inferred. The authors also acknowledge the UCLA Water Technology Research Center for providing computational facility support.

Supporting Information Available: The Supporting Information is available free of charge on the ACS Publications website at DOI: 10.1021/acsnano.5b04420.

Physicochemical properties and size distribution for the CeO_2 NPs, predicted fraction of settled CeO_2 NP mass, size distributions (histograms) for metal oxide NPs, fraction of settled NP mass calculated by the SP2N dosimetry model, settled metal oxide NPs based on UV–vis measurements, and dose–response curves (PDF)

REFERENCES AND NOTES

1. Guo, Z.; Tan, L. *Fundamentals and Applications of Nanomaterials*, 1st ed.; Artech House: Boston, 2009.
2. The Wilson Center. Inventory Finds Increase in Consumer Products Containing Nanoscale Materials http://www.nanotechproject.org/cpi/ (accessed on July 1, 2015).
3. Colvin, V. L. The Potential Environmental Impact of Engineered Nanomaterials. *Nat. Biotechnol.* **2003**, *21*, 1166–1170.
4. Gerber, C.; Lang, H. P. How the Doors to the Nanoworld Were Opened. *Nat. Nanotechnol.* **2006**, *1*, 3–5.
5. Scown, T. M.; Van Aerle, R.; Tyler, C. R. Review: Do Engineered Nanoparticles Pose a Significant Threat to the Aquatic Environment? *Crit. Rev. Toxicol.* **2010**, *40*, 653–670.
6. Nel, A.; Xia, T.; Mädler, L.; Li, N. Toxic Potential of Materials at the Nanolevel. *Science (Washington, DC, U. S.)* **2006**, *311*, 622–627.
7. Sharifi, S.; Behzadi, S.; Laurent, S.; Laird Forrest, M.; Stroeve, P.; Mahmoudi, M. Toxicity of Nanomaterials. *Chem. Soc. Rev.* **2012**, *41*, 2323–2343.
8. Jiang, W.; Kim, B. Y. S.; Rutka, J. T.; Chan, W. C. W. Nanoparticle-Mediated Cellular Response Is Size-Dependent. *Nat. Nanotechnol.* **2008**, *3*, 145–150.
9. Kahru, A.; Dubourguier, H.-C. From Ecotoxicology to Nanoecotoxicology. *Toxicology* **2010**, *269*, 105–119.
10. Wang, X.; Xia, T.; Ntim, S. A.; Ji, Z.; Lin, S.; Meng, H.; Chung, C.-H.; George, S.; Zhang, H.; Wang, M.; et al. Dispersal State of Multiwalled Carbon Nanotubes Elicits Profibrogenic Cellular Responses That Correlate with Fibrogenesis Biomarkers and Fibrosis in the Murine Lung. *ACS Nano* **2011**, *5*, 9772–9787.
11. Asharani, P. V.; Lianwu, Y.; Gong, Z.; Valiyaveettil, S. Comparison of the Toxicity of Silver, Gold and Platinum Nanoparticles in Developing Zebrafish Embryos. *Nanotoxicology* **2011**, *5*, 43–54.
12. Hardman, R. A Toxicologic Review of Quantum Dots: Toxicity Depends on Physicochemical and Environmental Factors. *Environ. Health Perspect.* **2006**, *114*, 165–172.
13. Zhang, H.; Ji, Z.; Xia, T.; Meng, H.; Low-Kam, C.; Liu, R.; Pokhrel, S.; Lin, S.; Wang, X.; Liao, Y.-P.; et al. Use of Metal Oxide Nanoparticle Band Gap to Develop a Predictive Paradigm for Oxidative Stress and Acute Pulmonary Inflammation. *ACS Nano* **2012**, *6*, 4349–4368.
14. Cohen, Y.; Rallo, R.; Liu, R.; Liu, H. H. In Silico Analysis of Nanomaterials Hazard and Risk. *Acc. Chem. Res.* **2013**, *46*, 802–812.
15. De Jong, W. H.; Borm, P. J. A. Drug Delivery and Nanoparticles: Applications and Hazards. *Int. J. Nanomed.* **2008**, *3*, 133–149.

16. Cattaneo, A. G.; Gornati, R.; Sabbioni, E.; Chiriva-Internati, M.; Cobos, E.; Jenkins, M. R.; Bernardini, G. Nanotechnology and Human Health: Risks and Benefits. *J. Appl. Toxicol.* **2010**, *30*, 730–744.
17. Damoiseaux, R.; George, S.; Li, M.; Pokhrel, S.; Ji, Z.; France, B.; Xia, T.; Suarez, E.; Rallo, R.; Mädler, L.; et al. No Time to Lose--High Throughput Screening to Assess Nanomaterial Safety. *Nanoscale* **2011**, *3*, 1345–1360.
18. Wiesner, M. R.; Lowry, G. V.; Alvarez, P.; Dionysiou, D.; Biswas, P. Assessing the Risks of Manufactured Nanomaterials. *Environ. Sci. Technol.* **2006**, *40*, 4336–4345.
19. Linkov, I.; Bates, M. E.; Canis, L. J.; Seager, T. P.; Keisler, J. M. A Decision-Directed Approach for Prioritizing Research into the Impact of Nanomaterials on the Environment and Human Health. *Nat. Nanotechnol.* **2011**, *6*, 784–787.
20. Xia, T.; Malasarn, D.; Lin, S.; Ji, Z.; Zhang, H.; Miller, R. J.; Keller, A. A.; Nisbet, R. M.; Harthorn, B. H.; Godwin, H. A.; et al. Implementation of a Multidisciplinary Approach to Solve Complex Nano EHS Problems by the UC Center for the Environmental Implications of Nanotechnology. *Small* **2013**, *9*, 1428–1443.
21. Shaw, S. Y.; Westly, E. C.; Pittet, M. J.; Subramanian, A.; Schreiber, S. L.; Weissleder, R. Perturbational Profiling of Nanomaterial Biologic Activity. *Proc. Natl. Acad. Sci. U. S. A.* **2008**, *105*, 7387–7392.
22. Krewski, D.; Acosta, D.; Andersen, M.; Anderson, H.; Bailar, J. C.; Boekelheide, K.; Brent, R.; Charnley, G.; Cheung, V. G.; Green, S.; et al. Toxicity Testing in the 21st Century: A Vision and a Strategy. *J. Toxicol. Environ. Health, Part B* **2010**, *13*, 51–138.
23. George, S.; Pokhrel, S.; Xia, T.; Gilbert, B.; Ji, Z.; Schowalter, M.; Rosenauer, A.; Damoiseaux, R.; Bradley, K. A.; Mädler, L.; et al. Use of a Rapid Cytotoxicity Screening Approach to Engineer a Safer Zinc Oxide Nanoparticle through Iron Doping. *ACS Nano* **2010**, *4*, 15–29.
24. Lin, S.; Zhao, Y.; Xia, T.; Meng, H.; Ji, Z.; Liu, R.; George, S.; Xiong, S.; Wang, X.; Zhang, H.; et al. High Content Screening in Zebrafish Speeds up Hazard Ranking of Transition Metal Oxide Nanoparticles. *ACS Nano* **2011**, *5*, 7284–7295.
25. Wittmaack, K. In Search of the Most Relevant Parameter for Quantifying Lung Inflammatory Response to Nanoparticle Exposure: Particle Number, Surface Area, or What? *Environ. Health Perspect.* **2006**, *115*, 187–194.
26. Teeguarden, J. G.; Hinderliter, P. M.; Orr, G.; Thrall, B. D.; Pounds, J. G. Particokinetics in Vitro: Dosimetry Considerations for in Vitro Nanoparticle Toxicity Assessments. *Toxicol. Sci.* **2006**, *95*, 300–312.
27. Cho, E. C.; Zhang, Q.; Xia, Y. The Effect of Sedimentation and Diffusion on Cellular Uptake of Gold Nanoparticles. *Nat. Nanotechnol.* **2011**, *6*, 385–391.
28. Park, M. S.; Park, J.; Jeon, S. K.; Yoon, T. H. The Effects of Sedimentation and Dissolution on the Cytotoxicity of Ag Nanoparticles. *J. Nanosci. Nanotechnol.* **2013**, *13*, 7264–7270.
29. Yoon, D.; Woo, D.; Kim, J.; Kim, M.; Kim, T.; Hwang, E.-S.; Baik, S. Agglomeration, Sedimentation, and Cellular Toxicity of Alumina Nanoparticles in Cell Culture Medium. *J. Nanopart. Res.* **2011**, *13*, 2543–2551.
30. Sharma, G.; Kodali, V.; Gaffrey, M.; Wang, W.; Minard, K. R.; Karin, N. J.; Teeguarden, J. G.; Thrall, B. D. Iron Oxide Nanoparticle Agglomeration Influences Dose Rates and Modulates Oxidative Stress-Mediated Dose-Response Profiles in Vitro. *Nanotoxicology* **2014**, *8*, 663–675.
31. Pal, A. K.; Bello, D.; Cohen, J.; Demokritou, P. Implications of in Vitro Dosimetry on Toxicological Ranking of Low Aspect Ratio Engineered Nanomaterials. *Nanotoxicology* **2015**, 1–15.
32. Summers, M. R. B.; Brown, M. R.; Hondow, N.; Brydson, R.; Rees, P.; Brown, A. P. Statistical Prediction of Nanoparticle Delivery: From Culture Media to Cell. *Nanotechnology* **2015**, *26*, 155101.
33. Cohen, J.; Deloid, G.; Pyrgiotakis, G.; Demokritou, P. Interactions of Engineered Nanomaterials in Physiological Media and Implications for in Vitro Dosimetry. *Nanotoxicology* **2013**, *7*, 417–431.
34. Cohen, J. M.; Teeguarden, J. G.; Demokritou, P. An Integrated Approach for the in Vitro Dosimetry of Engineered Nanomaterials. *Part. Fibre Toxicol.* **2014**, *11*, 20.
35. Deloid, G.; Cohen, J. M.; Darrah, T.; Derk, R.; Rojanasakul, L.; Pyrgiotakis, G.; Wohlleben, W.; Demokritou, P. Estimating the Effective Density of Engineered Nanomaterials for in Vitro Dosimetry. *Nat. Commun.* **2014**, *5*, 3514.
36. Hinderliter, P. M.; Minard, K. R.; Orr, G.; Chrisler, W. B.; Thrall, B. D.; Pounds, J. G.; Teeguarden, J. G. ISDD: A Computational Model of Particle Sedimentation, Diffusion and Target Cell Dosimetry for in Vitro Toxicity Studies. *Part. Fibre Toxicol.* **2010**, *7*, 36.
37. Liu, R.; Zhang, H. Y.; Ji, Z. X.; Rallo, R.; Xia, T.; Chang, C. H.; Nel, A.; Cohen, Y. Development of Structure-Activity Relationship for Metal Oxide Nanoparticles. *Nanoscale* **2013**, *5*, 5644–5653.
38. Ji, Z.; Jin, X.; George, S.; Xia, T.; Meng, H.; Wang, X.; Suarez, E.; Zhang, H.; Hoek, E. M. V; Godwin, H.; et al. Dispersion and Stability Optimization of TiO2 Nanoparticles in Cell Culture Media. *Environ. Sci. Technol.* **2010**, *44*, 7309–7314.
39. Zook, J. M.; Rastogi, V.; MacCuspie, R. I.; Keene, A. M.; Fagan, J. Measuring Agglomerate Size Distribution and Dependence of Localized Surface Plasmon Resonance Absorbance on Gold Nanoparticle Agglomerate Size Using Analytical Ultracentrifugation. *ACS Nano* **2011**, *5*, 8070–8079.
40. Zook, J. M.; MacCuspie, R. I.; Locascio, L. E.; Halter, M. D.; Elliott, J. T. Stable Nanoparticle Aggregates/agglomerates of Different Sizes and the Effect of Their Size on Hemolytic Cytotoxicity. *Nanotoxicology* **2011**, *5*, 517–530.
41. Li, X.; Logan, B. E. Collision Frequencies of Fractal Aggregates with Small Particles by Differential Sedimentation. *Environ. Sci. Technol.* **1997**, *31*, 1229–1236.
42. Johnson, C. P.; Li, X.; Logan, B. E. Settling Velocities of Fractal Aggregates. *Environ. Sci. Technol.* **1996**, *30*, 1911–1918.
43. Li, X. Y.; Logan, B. E. Permeability of Fractal Aggregates. *Water Res.* **2001**, *35*, 3373–3380.
44. Liu, R.; Rallo, R.; George, S.; Ji, Z.; Nair, S.; Nel, A. E.; Cohen, Y. Classification NanoSAR Development for Cytotoxicity of Metal Oxide Nanoparticles. *Small* **2011**, *7*, 1118–1126.
45. Liu, H. H.; Surawanvijit, S.; Rallo, R.; Orkoulas, G.; Cohen, Y. Analysis of Nanoparticle Agglomeration in Aqueous Suspensions via Constant-Number Monte Carlo Simulation. *Environ. Sci. Technol.* **2011**, *45*, 9284–9292.
46. Liu, H. H.; Lanphere, J.; Walker, S.; Cohen, Y. Effect of Hydration Repulsion on Nanoparticle Agglomeration Evaluated via a Constant Number Monte--Carlo Simulation. *Nanotechnology* **2015**, *26*, 45708.
47. Hunter, R. J. *Foundations of Colloid Science*, 2nd ed.; Oxford University Press: New York, 2001.
48. Sheldon, K. F. *Smoke, Dust, and Haze: Fundamentals of Aerosol Dynamics*, 2nd ed.; Oxford University Press: New York, 2000.
49. Quik, J. T. K.; Lynch, I.; Van Hoecke, K.; Miermans, C. J. H.; De Schamphelaere, K. A. C.; Janssen, C. R.; Dawson, K. A.; Stuart, M. A. C.; Van De Meent, D. Effect of Natural Organic Matter on Cerium Dioxide Nanoparticles Settling in Model Fresh Water. *Chemosphere* **2010**, *81*, 711–715.
50. Han, X.; Corson, N.; Wade-Mercer, P.; Gelein, R.; Jiang, J.; Sahu, M.; Biswas, P.; Finkelstein, J. N.; Elder, A.; Oberdörster, G. Assessing the Relevance of in Vitro Studies in Nanotoxicology by Examining Correlations between in Vitro and in Vivo Data. *Toxicology* **2012**, *297*, 1–9.
51. Ritz, C. Toward a Unified Approach to Dose-Response Modeling in Ecotoxicology. *Environ. Toxicol. Chem.* **2010**, *29*, 220–229.
52. Sampah, M. E. S.; Shen, L.; Jilek, B. L.; Siliciano, R. F. Dose-Response Curve Slope Is a Missing Dimension in the Analysis of HIV-1 Drug Resistance. *Proc. Natl. Acad. Sci. U. S. A.* **2011**, *108*, 7613–7618.
53. Walkey, C. D.; Olsen, J. B.; Song, F.; Liu, R.; Guo, H.; Olsen, W.; Cohen, Y.; Emili, A.; Chan, W. C. W. Protein Corona Fingerprinting Predicts the Cell Association of Gold Nanoparticles. *ACS Nano* **2014**, *8*, 2439–2455.

54. Lundqvist, M.; Stigler, J.; Elia, G.; Lynch, I.; Cedervall, T.; Dawson, K. A. Nanoparticle Size and Surface Properties Determine the Protein Corona with Possible Implications for Biological Impacts. *Proc. Natl. Acad. Sci. U. S. A.* **2008**, *105*, 14265–14270.
55. Liu, R.; Rallo, R.; Bilal, M.; Cohen, Y. Quantitative Structure-Activity Relationships for Cellular Uptake of Surface-Modified Nanoparticles. *Comb. Chem. High Throughput Screening* **2015**, *18*, 365–375.
56. Weissleder, R.; Kelly, K.; Sun, E. Y.; Shtatland, T.; Josephson, L. Cell-Specific Targeting of Nanoparticles by Multivalent Attachment of Small Molecules. *Nat. Biotechnol.* **2005**, *23*, 1418–1423.
57. Asati, A.; Santra, S.; Kaittanis, C.; Perez, J. M. Surface-Charge-Dependent Cell Localization and Cytotoxicity of Cerium Oxide Nanoparticles. *ACS Nano* **2010**, *4*, 5321–5331.
58. Xu, L.; Takemura, T.; Xu, M.; Hanagata, N. Toxicity of Silver Nanoparticles as Assessed by Global Gene Expression Analysis. *Mater. Express* **2011**, *1*, 74–79.
59. Mortensen, N. P.; Hurst, G. B.; Wang, W.; Foster, C. M.; Nallathamby, P. D.; Retterer, S. T. Dynamic Development of the Protein Corona on Silica Nanoparticles: Composition and Role in Toxicity. *Nanoscale* **2013**, *5*, 6372–6380.
60. Liu, R.; France, B.; George, S.; Rallo, R.; Zhang, H.; Xia, T.; Nel, A.; Bradley, K.; Cohen, Y. Association Rule Mining of Cellular Responses Induced by Metal and Metal Oxide Nanoparticles. *Analyst* **2014**, *139*, 943–953.
61. Rallo, R.; France, B.; Liu, R.; Nair, S.; George, S.; Damoiseaux, R.; Giralt, F.; Nel, A.; Bradley, K.; Cohen, Y. Self-Organizing Map Analysis of Toxicity-Related Cell Signaling Pathways for Metal and Metal Oxide Nanoparticles. *Environ. Sci. Technol.* **2011**, *45*, 1695–1702.
62. Lison, D.; Vietti, G.; van den Brule, S. Paracelsus in Nanotoxicology. *Part. Fibre Toxicol.* **2014**, *11*, 35.
63. Song, C.; Wang, P.; Makse, H. A. A Phase Diagram for Jammed Matter. *Nature* **2008**, *453*, 629–632.
64. Rogak, S. N.; Flagan, R. C. Stokes Drag on Self-Similar Clusters of Spheres. *J. Colloid Interface Sci.* **1990**, *134*, 206–218.
65. Lee, D. J.; Chen, G. W.; Liao, Y. C.; Hsieh, C. C. On the Free-Settling Test for Estimating Activated Sludge Floc Density. *Water Res.* **1996**, *30*, 541–550.
66. Veerapaneni, S.; Wiesner, M. R. Hydrodynamics of Fractal Aggregates with Radially Varying Permeability. *J. Colloid Interface Sci.* **1996**, *177*, 45–57.
67. Woodfield, D.; Bickert, G. An Improved Permeability Model for Fractal Aggregates Settling in Creeping Flow. *Water Res.* **2001**, *35*, 3801–3806.
68. Gmachowski, L. Transport Properties of Fractal Aggregates Calculated by Permeability. *Colloids Surf., A* **2003**, *215*, 173–179.
69. Fröhlich, E.; Bonstingl, G.; Höfler, A.; Meindl, C.; Leitinger, G.; Pieber, T. R.; Roblegg, E. Comparison of Two in Vitro Systems to Assess Cellular Effects of Nanoparticles-Containing Aerosols. *Toxicol. In Vitro* **2013**, *27*, 409–417.
70. Nymark, P.; Jensen, K.; Suhonen, S.; Kembouche, Y.; Vippola, M.; Kleinjans, J.; Catalan, J.; Norppa, H.; van Delft, J.; Briede, J. Free Radical Scavenging and Formation by Multi-Walled Carbon Nanotubes in Cell Free Conditions and in Human Bronchial Epithelial Cells. *Part. Fibre Toxicol.* **2014**, *11*, 4.